

Novel Deep Learning Model for Predicting Wind Velocity and Power Estimation in Advanced INVELOX Wind Turbines

K. Ramesh Kumar[†] and M. Selvaraj

Mechanical Engineering Department, Sri Sivasubramaniya Nadar College of Engineering, Anna University, Chennai, India

[†]Corresponding Author Email: krameshkumarphd@mech.ssn.edu.in

(Received November 5, 2022; accepted February 21, 2023)

ABSTRACT

Wind energy is a renewable energy source that has grown rapidly in recent decades. This energy is converted into electricity using advanced INVELOX wind turbines. However, the wind velocity is critical, and predicting this velocity in real-time is challenging. As a result, a deep learning (DL) model has been developed to predict the velocity in advanced wind turbines using a novel enhanced Long Short-Term Memory (LSTM) model. The LSTM enhancement is executed by employing the Black Widow optimization with Mayfly optimization in the Python platform as application software. The dataset has been prepared using Ansys Fluent fluid flow analysis. In addition to that, the wind turbine power generation was computed analytically. A subsonic wind tunnel test is also performed by employing a 3-Dimensional printed physical model to validate the simulation dataset for this innovative design. The proposed MFBW-LSTM model (Enhanced LSTM with BWO and MFO) predicts efficiently, with an accuracy of 95.34%. Furthermore, the performance of the proposed model is compared to LSTM, BW-LSTM, and MF-LSTM. Accuracy, MAE, MAPE, MSE, and RMSE are among the performance criteria the proposed DL model achieves efficiently. As a result, the proposed DL model is best suited for velocity prediction of an Advanced INVELOX wind turbine in various cross sections with high accuracy.

Keywords: Deep learning; Advanced INVELOX wind turbine; Long short-term memory; Black widow optimization; Mayfly optimization; Python; Velocity prediction.

NOMENCLATURE

| | | | |
|---------|------------------------------------|-----------------|--|
| BOA | Black Widow Optimization Algorithm | PLA | Poly Lactic Acid Material |
| BW-LSTM | Enhanced LSTM with BWO | MAE | Mean Absolute Error |
| CAD | Computer-Aided Design | MAPE | Mean Absolute Percentage Error |
| CFD | Computational Fluid Dynamics | MOA | Mayfly Optimization Algorithm |
| DL | Deep Learning | MF-LSTM | Enhanced LSTM with MFO |
| DAWT | Diffuser Augmented Wind Turbine | MFBW-LSTM | Enhanced LSTM with BWO and MFO |
| FDM | Fused Deposition Modeling | RMSE | Root Mean Square Error |
| GUI | Graphical User Interface | RNN | Recurrent Neural Network |
| LSTM | Long Short-Term Memory | SST K- ω | Shear Stress Transport K- ω model |

1. INTRODUCTION

Wind energy is abundant, pollution-free, locally available, and renewable (Shahbazi *et al.* 2019). The stochastic nature of the wind is a continual

difficulty for the wind power generation industry; therefore, the prediction of power is incertitude (Zhu *et al.* 2021). Nowadays, wind energy is the fastest-growing energy source in the world due to freely existing unlimited wind and ecological ways to make electricity (Guo *et al.* 2019). According to the developed mean wind speed data, wind energy

rises in winter and reduction in fall (Ohba 2019). Many fields, including meteorology, environmental science, and aerospace, are critical for measuring wind velocity. This wind speed is transformed into wind power with the help of wind turbines and the predictions of the wind velocity are examined using the Neural Network model (Allison et al. 2019).

There are many wind speed forecasting methods have been developed. Physical laws and meteorological parameters are utilized by the physical approaches to construct mathematical models for predicting wind power. These approaches need a significant computational time which is not appropriate for short-term prediction. Deep learning, isolated forest, and enhanced models are used to predict wind power (Zi et al. 2020). Machine learning models in the wind speed series are powerful, with excellent generalization competence to simulate dynamic behavior (Allison et al. 2020). Artificial neural network (ANN), Elman neural network (ENN), Support vector machine (SVM), and Autoregressive moving average model (ARMA) are more advanced models (Li et al. 2021). Traditional machine learning models predict the wind speed using a single or multiple data sets. These methods are frequently applied for the precise tendency wind speed data. Moreover, with the growth of deep learning models, they are increasingly used for the wind speed prediction problem (Liu et al. 2018). To study the forecasting problem, commonly used deep neural networks are LSTM, restricted Boltzmann machine (RBM), auto-encoders, and the convolutional neural network (CNN) (Liu, Y. et al. 2020).

DAWT is used to harvest more power from the source. Also, due to low-pressure regions, flanged DAWT draws more wind through rotors than a bare wind turbine (Alpman 2018). As a result, the diffuser's attainable wind speed in DAWT is enhanced to generate high power output (Khodayar and Wang 2018). Furthermore, the INVELOX (increased velocity) wind turbine captures the wind from all directions and accelerates it with good turbine efficiency (Allaei and Andreopoulos 2014). Moreover, various INVELOX models with venture design and their velocity contours were examined by CFD (Gohar et al. 2019). As a result, the Advanced INVELOX design used a novel prediction model to predict the Velocity in different areas. Here, the enhanced LSTM is employed for the prediction process, and the LSTM is upgraded using Black widow optimization with the Mayfly optimization algorithm. Moreover, the power calculation is also performed by applying the wind turbine power estimation equation.

This article is systematically arranged as follows, section 2 analyses the research articles; section 3 discusses the research gaps in the surveyed articles; section 4 explains the proposed model and methodology of the system; section 5 describes the results obtained from the implementation process, performance evaluation, and comparative analysis; and the final section concludes this work.

2. LITERATURE SURVEY

Wind power can be predicted using a high-frequency SCADA (Supervisory Control and Data Acquisition) database with a 1-s sampling rate developed by a deep-learning neural network. Input features were constructed based on the physical process of offshore wind turbines, and its linear relationship was explored using Pearson product-moment correlation coefficients. The non-linear correlations were examined utilizing DL approaches (Lin and Liu 2020). The training-based method was developed for wind turbine blade stiffness prediction under fatigue testing using time series stiffness data. The residual stiffness of the blade fatigue life related to fatigue testing is found by combining the ancient fatigue data with a deep learning algorithm incorporating a long-short term memory network, hybrid network, and convolutional neural network (Liu, H. et al. 2020). The hybrid principal component analysis method (PCA) and deep learning explain hidden patterns in wind data and estimate wind power.

Moreover, a Tensor Flow procedure employs an optimized deep learning algorithm to predict wind power from important characteristics precisely (Khan et al. 2019). The new short-term wind speed prediction model investigated relies on an error correction strategy, deep learning algorithm, and double ensemble. To decay the exact wind speed series, the entire ensemble decomposition of empirical mode with variational and adaptive noise decomposition is proper. The long-term and short-term memory features were found, and the appropriate prediction model for each sub-series was created using a long short-term memory neural network (Ma et al. 2020). An EEL (ELM, ENN, LSTM) - ELM is a two-layer nonlinear combination method established for short-term wind speed prediction issues. The initial layer focuses on Elman neural network (ENN), long short-term memory neural network (LSTM), and extreme learning machine (ELM) to individually predict wind speed by creating their merits of estimation speed (Chen et al. 2019).

A new hybrid strategy for multi-step ahead wind speed forecasting is observed based on a weighted regularized extreme learning machine (WRELM), three-phase signal decomposition (TPSD), and feature extraction (FE). The TPSD is suggested for the first time to regulate the complex and irregular natures of wind speed, and it includes fast ensemble empirical mode decomposition (FEEMD), variational mode decomposition (VMD), and seasonal separation algorithm (SSA) (Wang et al. 2018). Hybrid intelligent learning is studied based on an adaptive neuro-fuzzy inference system (ANFIS) for online estimation of effective wind speed from instant values of tip speed ratio (TSR), rotor speed, and mechanical power (Asghar and Liu 2018). Various combinations of recurrent Kalman filter (RKF), wavelet neural network (WNN), artificial neural network (ANN), and Fourier series (FS) are used for wind power and wind speed prediction (Aly 2020). To boost the accuracy

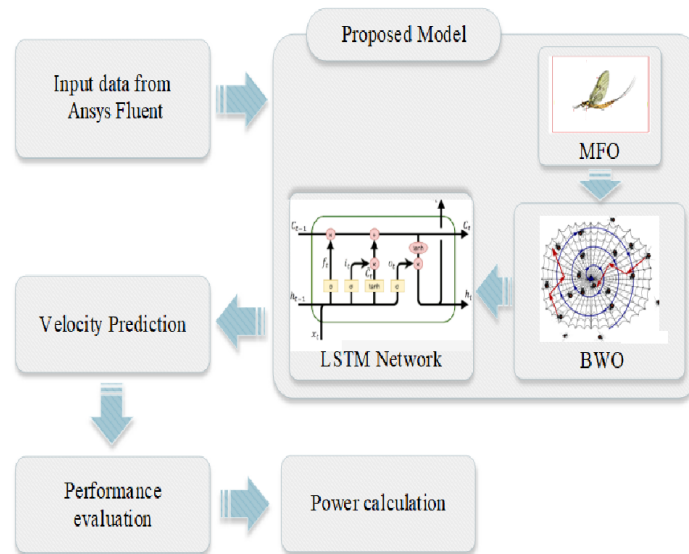


Fig. 1. Process flow structure of the proposed DL model.

of predicting the short-term wind speed, a hybrid wind speed prediction model is elucidated based on wavelet transform (WT), crow search algorithm (CSA), feature selection (FS) depending on entropy and mutual information (MI), and deep learning time series prediction depending on Long Short-Term Memory neural networks (LSTM) (Memarzadeh and Keynia 2020). Wind power is forecasted using Bi LSTM-CNN, and the results are compared to deep learning approaches such as Bi-LSTM, CNN, and LSTM-CNN (Hao *et al.* 2020).

3. LITERATURE GAP

The preceding section explored various methods for predicting wind velocity in turbines. Although the methodologies presented above perform well in prediction, several research gaps will be addressed in future studies. The proposed CNN-LSTM was shown to be efficient and capable of predicting from the raw stiffness data. Still, the required prediction level needs to be met an insufficient data sample (Liu *et al.* 2020). The proposed PCA with DL neural network technique attained a better accuracy level in the prediction process. The acquired findings needed fine parameter adjustment (Khan *et al.* 2019).

CEEMDAN and VMD techniques are used to increase the effect of the error correction approach. Still, an evolutionary algorithm's attained result accuracy is not the best result (Ma *et al.* 2020). Therefore, EEL-ELM can achieve better prediction performance. Still, an evolutionary algorithm's attained result accuracy is not the best result (Chen *et al.* 2019). The intended ANFIS was executed to forecast the values. But the required degree of accuracy was not attained (Asghar and Liu 2018). The section above outlined the various approaches utilized in wind speed prediction. The above-discussed methods can be used in the prediction of the velocity of the wind. However, several research gaps are indicated in future works.

4. PROPOSED METHODOLOGY

This section discusses the proposed model for predicting the wind velocity and power calculation for Advanced INVELOX Wind Turbine. For the prediction process, the proposed model combines enhanced LSTM with improved BOA, which is augmented by employing MOA, and a power equation is utilized for power determination. Figure 1 depicts the workflow of the proposed work.

4.1 Data Acquisition

The data for this task is collected from the Ansys Fluent study of the proposed Advanced INVELOX wind turbine. Firstly, the model is created in Solidworks software using the proposed Advanced INVELOX design, also called as Integrated Omni-directional Intake funnel, Natural fan, Straight diffuser, Splitter, and Flange (I²NS²F) model, and its critical dimensions are illustrated in Fig. 2. The CAD geometry is then transferred to Ansys Fluent for fluid flow analysis. The grid consistency test is conducted for three different grid densities to determine the optimum grid size such that the solution is consistent regardless of the grid. A free stream velocity of 5.5m/s is considered at the inlet. Because of the usual environmental conditions, the ambient pressure is assumed at the intake hopper and exit splitter. Also, a medium-turbulence (5%) is suggested for this simulation study (Ramesh and Selvaraj 2023). A pressure-based solver was used due to its adaptability for a wide range of flow phases (Sorribes-Palmer *et al.* 2017). The SST K- ω turbulence model was employed in this investigation. It is more accurate and efficient for airfoils, adverse pressure gradient flows, nearby walls, and faraway regions. Furthermore, by including transport effects in the eddy-viscosity formulation, this model accounts for the transit of turbulence kinetic energy and gives accurate

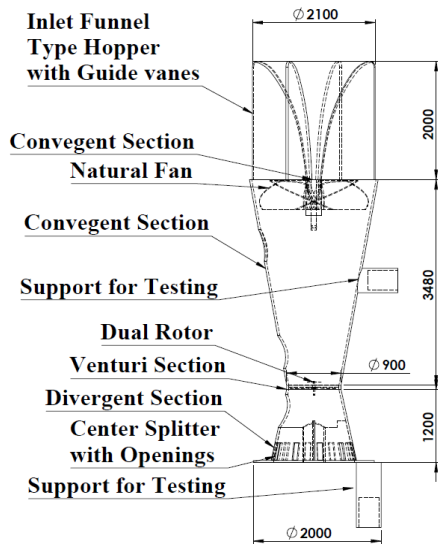


Fig. 2. Critical dimensions of Advanced INVELOX wind turbine.

estimates of the beginning and extent of flow separation under detrimental pressure gradients (Kosasih and Hudin 2016).

The velocity contour obtained from the flow study is illustrated in Fig. 3. The flow simulation is performed for various input velocities, and the results are attained at different cross-sectional areas of the Inlet hopper, Natural fan, Convergent section, Turbine entry, Turbine exit, Divergent section, and Exit splitter (Ramesh and Selvaraj 2023). The power law velocity profile equation is utilized for the velocity estimation, and it is derived below,

$$v(h) = v_{ref} \left(\frac{h}{h_{ref}} \right)^\alpha \quad (1)$$

Where $v(h)$ represents the velocity at height h , v_{ref} represents the input velocity, h represents the height of vertical ordinate, h_{ref} represents the height at reference area, and α is the tuning parameter generally set to 1/7. Furthermore, the obtained values are noted as a dataset for the velocity prediction process, and these data are sent to the enhanced LSTM network.

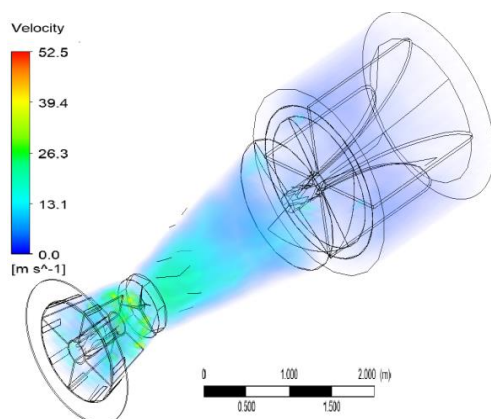


Fig. 3. Flow analysis velocity contour.

4.2 Data Validation

The experiment data for this DL model is measured from the wind tunnel testing of a 3-Dimensional printed miniature model of the Advanced INVELOX wind turbine. Due to the limited dimensions of the wind tunnel test section and the enormous blockage, testing real-scale wind turbine systems with massive rotors in a wind tunnel is usually impossible. Therefore, the Advanced INVELOX design is scaled down for 3D printing based on tunnel blockages (Howell *et al.* 2010).

4.2.1 3D Printing of Physical Model

The method of creating 3D physical models from digital files is known as 3D printing. First, a 3D model was created in Solidworks CAD software and converted to the STL (Stereolithography) file format. Then, printing layers of a particular material manufacture the entire design on top of one another by the FDM technique. This is one of the fastest processes for producing complex products in the shortest time without using complicated manufacturing processes or large machines. PLA materials were chosen for use with the 3D printed wind turbine model described herein because of its low cost, high availability, reliability, and limited printer needs. (Bassett *et al.* 2015). The 3D manufactured product for wind turbine design in the Ender 3D printing FDM machine is shown in Fig. 4.

4.2.2 Wind Tunnel Testing

Geometric scaling is considered in this design for subsonic wind tunnel testing (Manwell *et al.* 2009). Scaling is done by the available wind tunnel testing facilities. 3D printed miniature physical model is



Fig. 4. 3D printed physical model.



Fig. 5. Experimental setup in Wind tunnel Layout.

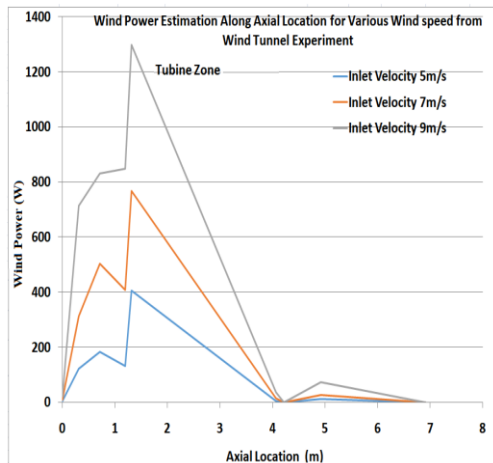


Fig. 6. Wind power estimation for various wind speeds at Wind tunnel Layout.

placed in the 300mmX200mmX1000mm of the test volume, as indicated in Fig. 5. The wind tunnel was operated at multiple speeds. All input and critical section venturi plane velocity results were taken using an Equinox digital anemometer for each speed increase. The velocity at the test ports were measured, and wind power was plotted for three different input wind speeds, as shown in Fig. 6.

As a result, the Advanced INVELOX design achieved a venturi section wind speed of 26m/s for 5m/s input wind speed in the wind tunnel. When compared to the numerical simulation, there is approximately 37% variation. However, it achieved a closer result with theoretical computations. Scaling down rotating machinery always results in efficiency losses, which can be expected (Deam 2008; Akour and Bataineh 2019).

4.2.2 Long Short-Term Memory (LSTM)

LSTM network is the advanced model of RNN because it cannot retrieve long-term memories. However, LSTM can store long-term and short-term data with the help of a memory cell unit. Moreover, the LSTM operates on three gates; the input gate, the output gate, and the forget gate. First, the input gate feeds the past and present timeline data to the hidden layer. Next, forget gate was performed, and attained the necessary data for further process.

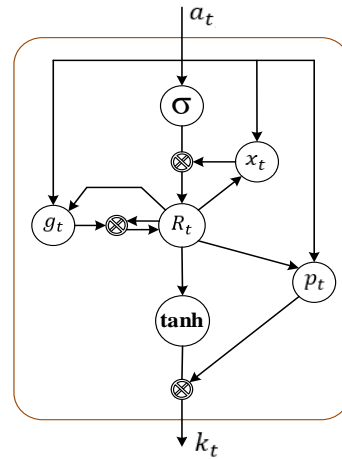


Fig. 7. Block diagram for the LSTM.

Finally, the output gate stores the current data and feeds it into the additional layer. As illustrated in Fig. 7, the memory cell in the block is governed by the presented gates.

Let us consider the input sequence as (a_1, a_2, \dots, a_n) and the hidden layer state is regarded as (m_1, m_2, \dots, m_n) , therefore the equations for estimating each gate function values at time t are given below,

$$x_t = \sigma(s_x k_{t-1} + u_x a_t) \quad (2)$$

$$g_t = \sigma(s_g k_{t-1} + u_g a_t) \quad (3)$$

$$R_t = g_t \times R_{t-1} + x_t \times \tanh(s_R k_{t-1} + u_R a_t) \quad (4)$$

$$p_t = \sigma(s_p k_{t-1} + u_p a_t + v_p R_t) \quad (5)$$

$$k_t = p_t \times \tanh(R_t) \quad (6)$$

Where x_t represents the input value, k_{t-1} denotes the output of the previous layer, a_t designates the current input at time t , g_t represents the forget gate value, R_t denotes the memory cell, and p_t specifies the output gate value. In addition to that, k_t represents the output of the block, and $s, u,$ and v express the weight bias. Here, σ and \tanh are taken as the activation function.

4.2.2 Black Widow Optimization Algorithm (BOA)

BOA is based on the principle of the black widow spider's lifestyle. The spider's mating process is considered for the optimization process. The female spider commences the mating process by locating the precise place of her net using a pheromone to impress the male spider. The first one is sexual cannibalism which is offered to the fitness value of the male and female spider populations. Next is sibling cannibalism, which is used to increase the cannibalism rates by keeping the fittest young spiders in the population while rejecting others. The

third type is utilized based on the fitness value of the young spiders and the mother spider.

The black widow optimization process begins with a random initial black widow population. This random population includes female and male black widows for producing offspring for the next generation. The initial population of a black widow is defined in the equation,

$$X_{N,d} = [x_{1,1}x_{1,2}x_{1,3} \dots x_{1,d}] \tag{7}$$

Where $X_{N,d}$ denotes the black widow population, d denotes the number of decision variables, N indicates the population number, and ub represents the upper bound of the population. By using potential solution population ($X_{N,d}$) to maximize or minimize the objective function and it is defined as,

$$\text{Objective Function} = f(X_{N,d}) \tag{8}$$

In the BWO model, numerous predefined parameters are specific such as Q_{pt} , Q_e , R_p , R_E , Ω_{ts} , Ω_{es} , Ω_{er} , and Ω_{sr} , which are determined in the above section. Those parameters show the upper and lower bounds of P_e and P_s .

$\frac{Q_e - P_{pt}\Omega_{ts}}{\Omega_{es}}$ is the lower bound of P_e , $\frac{Q_p - P_{e,max}\Omega_{er}}{\Omega_{es}}$ is the upper bound of P_e , $\frac{Q_p - (Q_e - P_{pt}\Omega_{ts})\Omega_{er}/\Omega_{es}}{\Omega_{sr}}$ is the upper bound of P_s and $\frac{Q_p - P_{e,max}\Omega_{er}}{\Omega_{sr}}$ is the lower bound of P_s . The black widow mutation will be optimized in this stage, where the mutation rate is employed for selecting a young spider. A small random value is added to a determined young spider for the mutation process.

$$Z_{k,d} = Y_{k,d} + \alpha \tag{9}$$

Where $Z_{k,d}$ denotes the mutated population of black widows, $Y_{k,d}$ represents the randomly selected young spider, k indicates the randomly selected number, and α designates the random mutate value.

4.2.3 Mayfly Optimization Algorithm (MOA)

MOA is developed by combining genetic algorithm (GA), Particle swarm optimization (PSO), and Firefly Algorithm. This algorithm is performed based on the mating behavior of both male and female Mayflies. The male and female populations are initialized as $x = [x_1, \dots, x_d]$ and $y = [y_1, \dots, y_d]$, respectively. These populations are used to find the candidate solution for the d -dimensional vector. The MFO objective function is depicted below,

$$FF = \text{Optimal learning rate} \tag{10}$$

Furthermore, by utilizing the below equation, the corresponding velocity is calculated,

$$v = [v_1, \dots, v_d] \tag{11}$$

Here, $f(g_{best})$ represents the global best position, which is used to update the next iteration and calculate the cartesian distance between the global best agent g_{best} and the personal element. This statement is described by the equations below.

$$x_i^{t+1} = x_i^t + v_i^{t+1} \tag{12}$$

$$v_{ij}^{t+1} = v_{ij}^t + a_1 e^{-\beta r_g^2} (g_{bestj} - x_{ij}^t) + a_2 e^{-\beta r_p^2} (p_{bestj} - x_{ij}^t) \tag{13}$$

Where,

$x_{ij}^t \Rightarrow$ At the current iteration t , the agent i in dimension j ,

$v_{ij}^t \Rightarrow$ Velocity,

$a_1 \Rightarrow$ Global learning coefficient,

$a_2 \Rightarrow$ Personal learning coefficient,

$r_g \Rightarrow$ Cartesian distance for global,

$r_p \Rightarrow$ Cartesian distance for personal,

Furthermore, the finest agent's velocity for the current iteration is computed by applying the following equation,

$$v^{t+1} = v^t + d \times r \tag{14}$$

Where,

$d \Rightarrow$ Nuptial dance,

$r \Rightarrow$ Random variable located in $[-1,1]$.

The female Mayfly's movement velocity is then updated using the following equation, which is determined by accounting for the Cartesian distance between male and female Mayflies.

$$v_{ij}^{t+1} = \begin{cases} v_{ij}^t + a_3 e^{-\beta r_{mf}^2} (x_{ij}^t - y_{ij}^t), & \text{if } f(y_i) > f(x_i) \\ v_{ij}^t + fl \times r, & \text{if } f(y_i) \leq f(x_i) \end{cases} \tag{15}$$

Where,

$y \Rightarrow$ Female agent, $a_3 \Rightarrow$ Learning coefficient,

$\beta \Rightarrow$ Distance sight coefficient,

$r_{mf} \Rightarrow$ Cartesian distance between the female and male agent.

Following this assessment, the best female Mayfly selected the best male Mayfly for mating to produce offspring. A fraction of the created offspring is male, while the remaining are female. Finally, the weak solution is substituted by the best solution, reiterating the process until the desired best solution is attained.

4.3 Proposed Enhanced LSTM

This section explores developing the proposed enhanced LSTM for the velocity prediction process. Firstly, LSTM initializes the parameters for the

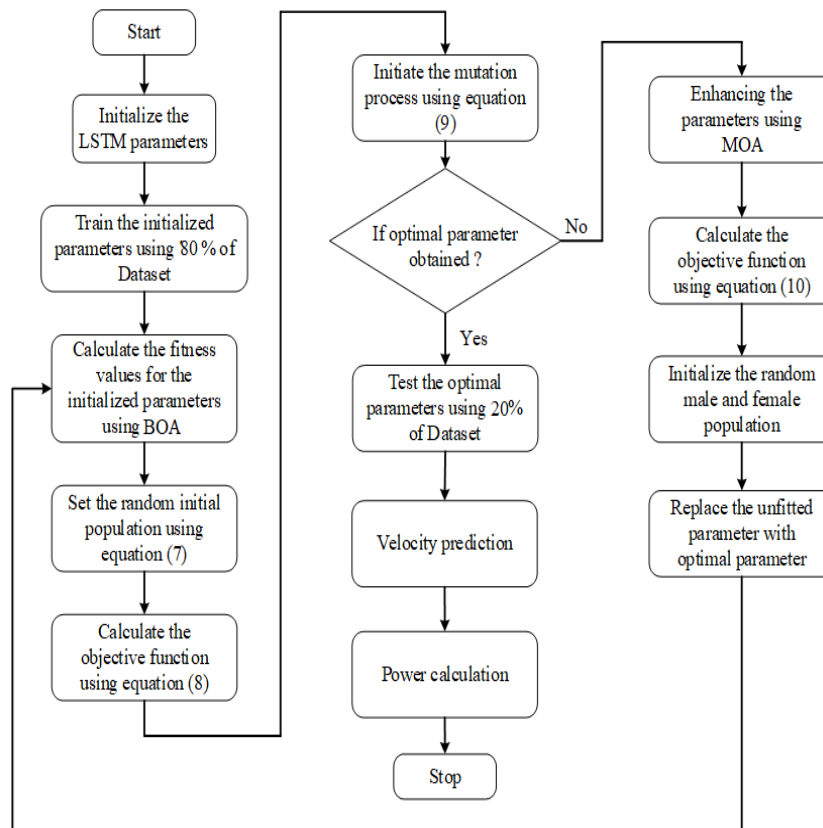


Fig. 8. Flowchart for the proposed DL Model.

input dataset and estimates the gate values as per the equations (2-6). The fitness value for the initialized parameters is then computed via BOA. BOA randomly initializes the population by utilizing equation (7). The objective function of the BOA is depicted in equation (8). The BOA uses equation (9) to perform the mutation process. The population is selected. As a result, this process and the fittest parameter are moved to the prediction process, while the parameters not being fit are moved to the MOA. The objective function of the MOA is estimated using equation (10) in this case. Then, the male and female Mayfly populations are initialized based on the parameters not being fit. The optimal parameter is selected from the initialized population. BWO then executes the process of estimating fitness values. This is an iterative process that continues until the optimal parameters are obtained. After attaining the optimal parameters, the velocity prediction process is performed. Once the velocity is predicted, the output value is fed to the performance evaluation. Then, the velocity value is taken for the calculation of power in each cross-sectional area of the proposed Advanced INVELOX wind turbine. The power is thus calculated by utilizing the below-derived formula,

$$p = \frac{1}{2} \rho \times A \times N_W \times N_G \times N_T \times v^3 \quad (16)$$

Where power is represented by P, wind density is denoted as ρ . The cross-sectional area is denoted as A, the whirlpool loss factor is defined as N_W , the

efficiency of the generator is expressed in N_G , the efficiency of the turbine is expressed in N_T , and the velocity of the wind is defined as V. The flow chart for the proposed deep learning model is illustrated in Fig. 8.

5. RESULTS AND DISCUSSION

This section presents the wind speed forecasting and wind power calculation findings for the advanced INVELOX wind turbine. MFBW-LSTM performs wind speed forecasting. Python 3.8.11 is used to develop the implementation program in the experimental process with the system configuration of the i3 9th generation intel core processor, 8GB RAM, and CPU speed of 3.6GHz. In the following section, the results of wind speed prediction and wind power generation are discussed and analyzed (Bekir and Resat 2019).

5.1 Wind speed forecasting and power calculation

During the implementation process, a GUI is developed in Python programming for the proposed DL model, which includes an input bar for obtaining the results based on the respective input value. The GUI output of wind speed and power for an input velocity of 5.5m/s is illustrated in Fig. 9. This proposed model can accept input values ranging from zero to 53m/s. It also displays a list of

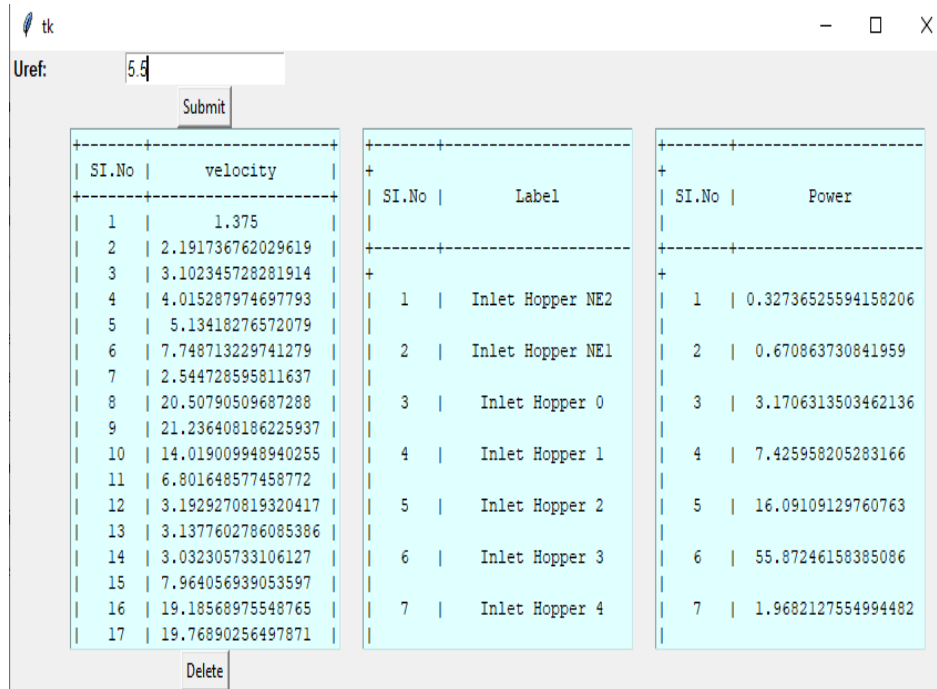


Fig. 9. GUI of developed application software for the proposed methodology.

Table 1 Plane label list of Advanced INVELOX Wind Turbine.

| Label No | Label | Label No | Label | Label No | Label |
|----------|---------------------|----------|------------------|----------|---------------------|
| 1 | Inlet Hopper NE2 | 14 | Natural Fan exit | 27 | Divergent 5 |
| 2 | Inlet Hopper NE1 | 15 | Converge 1 | 28 | Exit splitter 1 |
| 3 | Inlet Hopper 0 | 16 | Converge 2 | 29 | Exit splitter 2 |
| 4 | Inlet Hopper 1 | 17 | Converge 3 | 30 | Exit splitter 3 |
| 5 | Inlet Hopper 2 | 18 | Converge 4 | 31 | Exit splitter 4 |
| 6 | Inlet Hopper 3 | 19 | Converge 4.1 | 32 | Exit splitter 5 |
| 7 | Inlet Hopper 4 | 20 | Converge 5 | 33 | Exit split hole 1 |
| 8 | Natural Fan 0.29m | 21 | Converge 6 | 34 | Exit split hole 2 |
| 9 | Natural Fan | 22 | Turbine entry | 35 | Exit split hole 3 |
| 10 | Natural Fan 4 0.27m | 23 | Turbine exit | 36 | Exit split flange 1 |
| 11 | Natural Fan 1 0.26m | 24 | Divergent 1 | 37 | Exit split flange 2 |
| 12 | Natural Fan 3 0.255 | 25 | Divergent 2 | | ----- |
| 13 | Natural Fan 2 0.25m | 26 | Divergent 3 | | ----- |

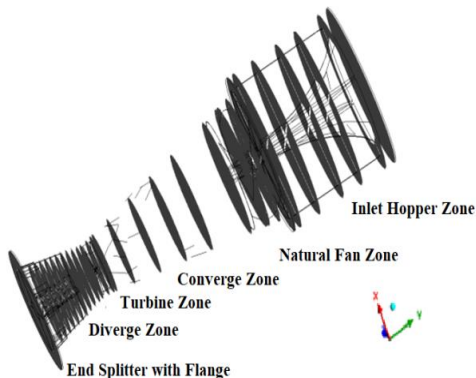


Fig. 10. Plane location at Flow analysis velocity contour.

velocity, label, and power values based on the input value. The plane details for various cross sections of the turbine system are given in Table 1, and their location in the design is shown in Fig. 10. (Few Planes are hidden for best visibility purposes).

The above graphs (Figs. 11 and 12) illustrate the power and velocity fluctuation for input velocity values of 5m/s and 7m/s. Here, the x-axis indicates the axial diffuser length denoted by the label shown in Table 1, while the y-axis indicates the power and velocity values. The variation of power and velocity are depicted in orange and blue colors, respectively.

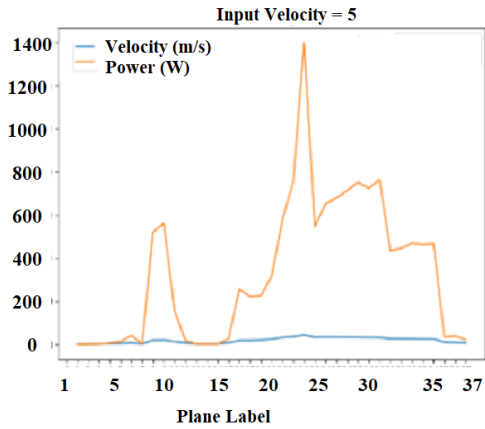


Fig. 11. Power and velocity variation on plane labels for input velocity 5 m/s.

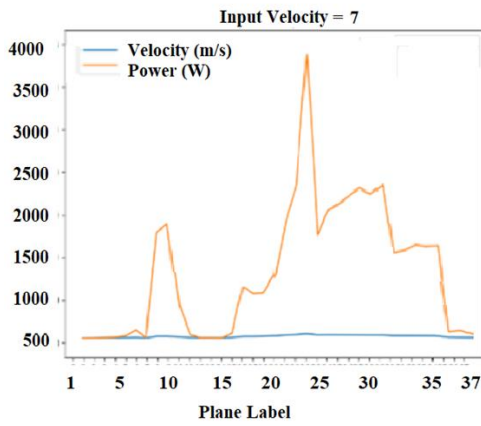


Fig. 12. Power and velocity variation for input velocity 7 m/s.

The wind power generation along the various axial locations of the Advanced INVELOX design is presented in Fig. 13 for 5m/s, 7m/s, and 9m/s. These graphs are proved that the power and velocity values are higher in the turbine entry area. Moreover, the performance evaluation was also conducted to validate the accuracy and error levels of the proposed DL model.

5.2 Performance Evaluation

The proposed MFBW-LSTM is validated using performance matrices like Accuracy, Loss, MAE, MAPE, MSE, and RMSE (Hao, W. et al. 2020). The formulae used to assess these performance matrices are presented below,

$$\text{Accuracy (A)} = \frac{\text{True Positive (TP)} + \text{True Negative (TN)}}{\text{Total Samples}} \quad (17)$$

$$\text{MSE} = \frac{1}{n} \sum_{t=1}^n (y_t - \tilde{y}_t)^2 \quad (18)$$

$$\text{MAE} = \frac{1}{n} \sum_{t=1}^n |y_t - \tilde{y}_t| \quad (19)$$

$$\text{RMSE} = \sqrt{\frac{1}{n} \sum_{t=1}^n (y_t - \tilde{y}_t)^2} \quad (20)$$

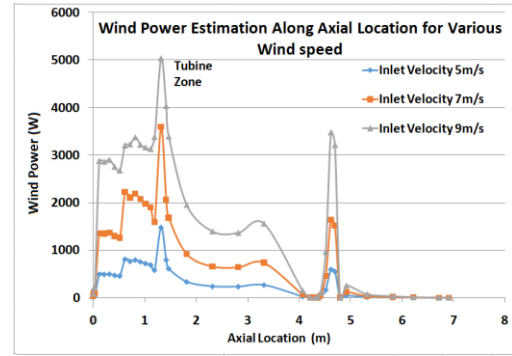


Fig. 13. Wind power production for the various input wind speed.

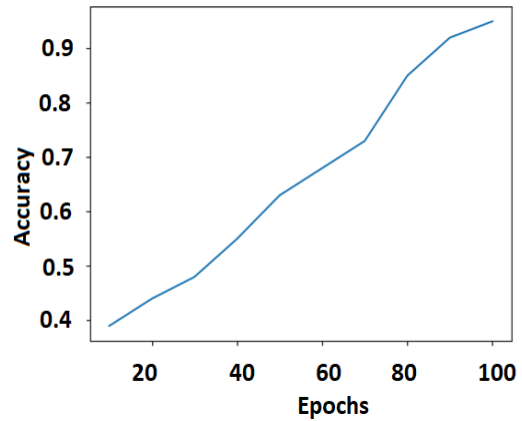


Fig. 14. Graphical representation for the accuracy of the proposed technique.

$$\text{MAPE} = \frac{100\%}{n} \sum_{t=1}^n \left| \frac{y_t - \tilde{y}_t}{y_t} \right| \quad (21)$$

Where,

TP => Model correctly predicts the presence of a condition or positive class,

TN => Model correctly predicts the absence of a condition or negative class,

n => Number of samples taken,

y_t => Measured wind speed,

\tilde{y}_t => Predicted wind speed.

The acquired accuracy for the proposed MFBW-LSTM is 95.34%, as illustrated in Fig. 14. The epoch value is set as 100 for the implementation process. Fig. 15 reveals that the proposed technique has an MAE of 26.08% at the 100th epoch. Similarly, the MAPE obtained for the proposed model is graphically verified in Fig.16, which indicates that it is 28.22% at the 100th epoch. Fig. 17 depicted the MSE for the proposed technique at the 100th epoch as 22.11%. In addition, Fig. 18 verified the RMSE of the proposed method and is obtained as 18.09 % at the 100th epoch for this technique. Therefore, as per the performance estimation, the proposed MFBW-LSTM DL model can predict wind velocity in advanced INVELOX wind turbines.

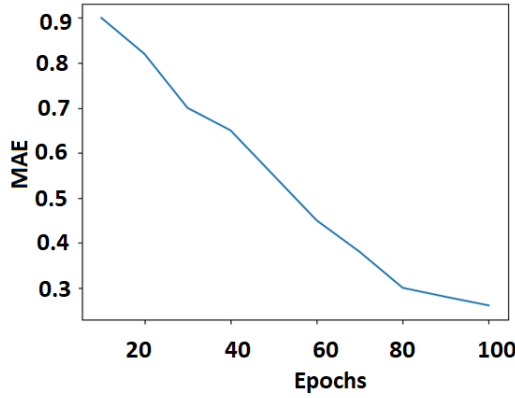


Fig. 15. Proposed technique – MAE.

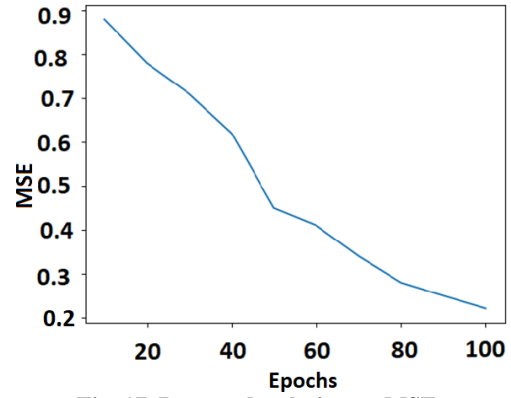


Fig. 17. Proposed technique – MSE.

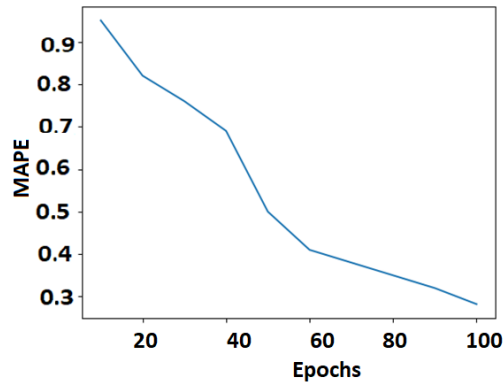


Fig. 16. Proposed technique – MAPE.

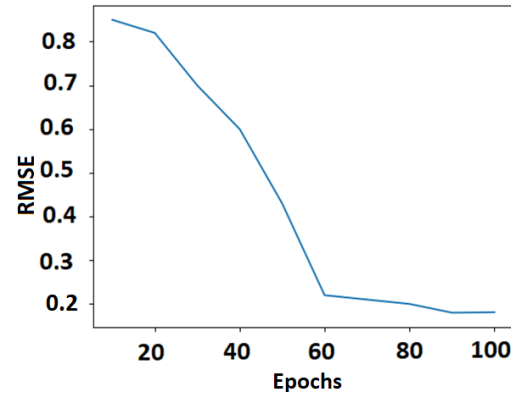


Fig. 18. Proposed technique – RMSE.

| Labels | | LSTM | BW-LSTM | MF-LSTM | MFBW-LSTM |
|--------|------------------|------------------|------------------|------------------|-------------------------|
| SI.No | Label | SI.No velocity | SI.No velocity | SI.No velocity | SI.No velocity |
| 1 | Inlet Hopper NE2 | 1 0.94604 | 1 1.00055 | 1 1.05343 | 1 1.25 |
| 2 | | 2 1.63809 | 2 1.72293 | 2 1.87150 | 2 1.992487965481472 |
| 3 | | 3 2.51547 | 3 2.54499 | 3 2.65004 | 3 2.8203142984381033 |
| 4 | | 4 3.20116 | 4 3.43395 | 4 3.49679 | 4 3.650261795179812 |
| 5 | | 5 4.25672 | 5 4.38956 | 5 4.53684 | 5 4.6674388779279905 |
| 6 | | 6 6.70912 | 6 6.84057 | 6 6.90327 | 6 7.044284754310254 |
| 7 | | 7 1.86390 | 7 2.05667 | 7 2.18367 | 7 2.3133896325560337 |
| 8 | Inlet Hopper NE1 | 8 18.28491 | 8 18.40181 | 8 18.44627 | 8 18.64355008066256 |
| 9 | | 9 18.92584 | 9 19.07245 | 9 19.13299 | 9 19.305825623841763 |
| 10 | Inlet Hopper 1 | 10 12.34566 | 10 12.53949 | 10 12.55324 | 10 12.744554499036596 |
| 11 | | 11 5.76519 | 11 5.95473 | 11 5.99473 | 11 6.183316888598883 |
| 12 | Inlet Hopper 2 | 12 2.51883 | 12 2.67799 | 12 2.78941 | 12 2.902660983574583 |
| 13 | | 13 2.52756 | 13 2.62639 | 13 2.66157 | 13 2.8525093441895804 |
| 14 | Inlet Hopper 3 | 14 2.28718 | 14 2.51855 | 14 2.65044 | 14 2.7566415755510243 |
| 15 | | 15 6.85736 | 15 7.03024 | 15 7.09872 | 15 7.240051762775997 |
| 16 | Inlet Hopper 4 | 16 17.12435 | 16 17.17759 | 16 17.27771 | 16 17.44153614135241 |
| 17 | | 17 17.63493 | 17 17.72074 | 17 17.85775 | 17 17.97172960452261 |

Fig. 19. GUI of Application software: Predicted velocity for the comparative analysis.

5.3 Comparative Analysis

This section provides the comparative analysis between the implemented MFBW-LSTM, LSTM, BW-LSTM, and MF-LSTM. The findings are summarized in Fig. 19 for an input velocity of

5.5m/s. The application software developed in Python (Fig. 19) demonstrates the predicted velocity for LSTM, BW-LSTM, MF-LSTM, and MFBW-LSTM. The predicted velocity in the proposed MFBW-LSTM is more appropriate when compared to other models such as LSTM, BW-

Table 2 Summary of the implemented techniques.

| Techniques | Accuracy (%) | MAE (%) | MAPE (%) | MSE (%) | RMSE (%) |
|------------|--------------|---------|----------|---------|----------|
| LSTM | 86.59 | 32.55 | 34.83 | 28.24 | 27.17 |
| BW-LSTM | 92.3 | 27.05 | 30.98 | 24.81 | 21.33 |
| MF-LSTM | 92.5 | 26.97 | 29.12 | 24.53 | 20.96 |
| MFBW-LSTM | 95.34 | 26.08 | 28.22 | 22.11 | 18.09 |

LSTM, and MF-LSTM. The values obtained for Accuracy, MAE, MAPE, MSE, and RMSE for the LSTM, BW-LSTM, MF-LSTM, and MFBW-LSTM are given in Table 2.

The LSTM model revealed 86.59, 32.55, 34.83, 28.24, and 27.17 % for the Accuracy, MAE, MAPE, MSE, and RMSE, respectively. The BW-LSTM model provided 92.3, 27.05, 30.98, 24.81, and 21.33 % for the acquired performance metrics. The MF-LSTM model obtained 92.5, 26.97, 29.12, 24.53, and 20.96 % for the performance metrics, respectively. In addition, the proposed MFBW-LSTM achieved 95.34, 26.08, 28.22, 22.11, and 18.09 % in respect to the Accuracy, MAE, MAPE, MSE, and RMSE.

The variations arrived at for the Accuracy, MAE, MAPE, MSE, and RMSE for the implemented techniques is depicted as a bar diagram in Fig. 20, 21, 22, 23, and 24, with the implemented techniques such as LSTM, BW-LSTM, MF-LSTM, and MFBW-LSTM in the x-axis and the performance index values in the y-axis. Fig. 20 proves that the proposed technique is more accurate than the other techniques. Figure 21 illustrates that the MAE of

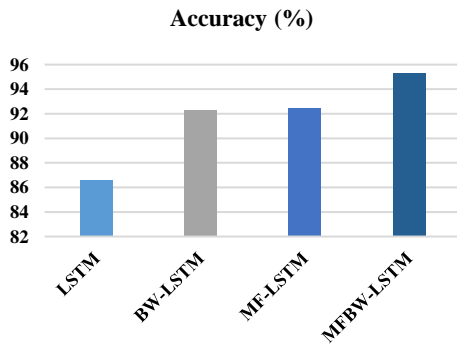


Fig. 20. Accuracy level for Implemented techniques.

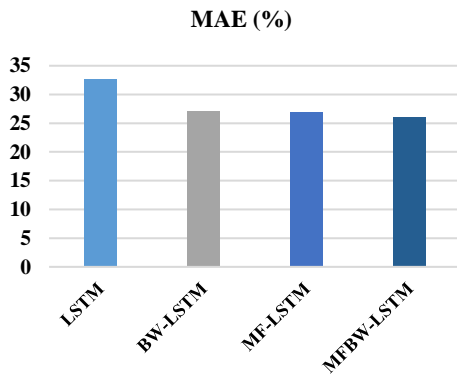


Fig. 21. Implemented techniques – MAE.

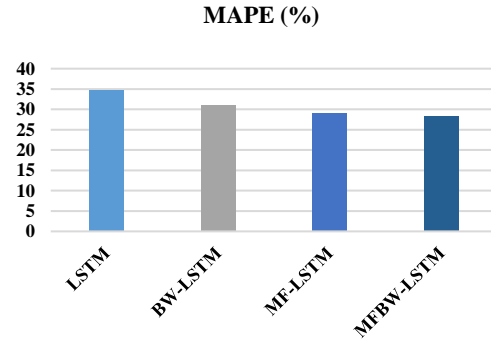


Fig. 22. Implemented techniques - MAPE

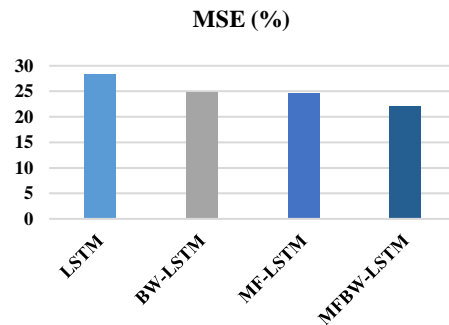


Fig. 23. Implemented techniques - MSE

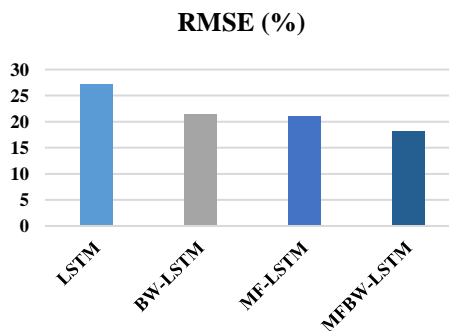


Fig. 24. Implemented techniques – RMSE.

the proposed techniques is achieved a lesser value when compared to the other implemented techniques. The bar diagram in Fig. 22 provides the minimum MAPE value for MFBW-LSTM when compared to the different techniques. From Fig.23, the proposed model has the lowest MSE value compared to the other techniques. Moreover, Fig. 24 reveals that the proposed MFBW-LSTM has the lowest RMSE value compared to the other techniques, such as LSTM, BW-LSTM, and MF-LSTM. Finally, the suggested MFBW-LSTM model

outperforms the implemented techniques in Accuracy, MAE, MAPE, MSE, and RMSE.

6. CONCLUSION

The main objective of this work is to produce a novel DL model for the velocity prediction in an Advanced INVELOX wind turbine. The developed DL model and its performance are given as follows,

- The prediction model is constructed by an enhanced LSTM which is upgraded with the help of improved BOA. The BOA is further enhanced by employing the MOA, and thus produces a innovative model called MFBW-LSTM.
- The power calculation comparison for a wind turbine is utilized for estimating the variation of power in the wind turbine based on predicted velocity.
- The dataset for the proposed model is developed from the Ansys Fluent fluid flow analysis of advanced INVELOX wind turbine design. In addition, the wind tunnel tests were performed on a downsized 3D printed low-weight model to obtain velocity contour along the axial direction of wind turbine design to validate these results. The DL implementation process is performed in the Python platform.
- The planned MFBW-LSTM is efficiently performed for the velocity prediction process with an accuracy level of 95%. Furthermore, the error metrics like MAE, MAPE, MSE, and RMSE are estimated to be 0.26, 0.28, 0.22, and 0.18, respectively.
- The power is also determined in various plane sections in the wind turbine. Moreover, the proposed MFBW-LSTM is compared with the LSTM, BW-LSTM, and MF-LSTM. The proposed technique is effectively performed in all performance metrics.
- The suggested MFBW-LSTM is most suitable and efficient for the velocity prediction and power calculation for green and clean energy production in Advanced INVELOX wind turbines.

ACKNOWLEDGMENTS

The research illustrated in this paper was performed at Sri Sivasubramaniya Nadar (SSN) College of Engineering, an Autonomous Institution, Anna University, Chennai, India. The facility and cooperation offered by the mechanical engineering team of SRM University, Chennai, India, to carry out the wind tunnel experiment is appreciated.

REFERENCES

Akour, S. N. and H. O. Bataineh (2019). Design considerations of wind funnel concentrator for low wind speed regions. *AIMS Energy* 7(6), 728-742.

Allaei, D. and Y. Andreopoulos (2014). INVELOX: Description of a new concept in wind power and its performance evaluation. *Energy* 69, 336-344.

Allison, S., H. Bai and B. Jayaraman (2019). Estimating wind velocity with a neural network using quadcopter trajectories. In *AIAA Scitech 2019 Forum*, p. 1596.

Allison, S., H. Bai and B. Jayaraman (2020). Wind estimation using quadcopter motion: A machine learning approach. *Aerospace Science and Technology* 98, 105699.

Alpman, E. (2018). Multiobjective aerodynamic optimization of a microscale ducted wind turbine using a genetic algorithm. *Turkish Journal of Electrical Engineering & Computer Sciences* 26(1), 618-629.

Aly, H. H. (2020). A novel deep learning intelligent clustered hybrid models for wind speed and power forecasting. *Energy* 213, 118773.

Asghar, A. B. and X. Liu (2018). Adaptive neuro-fuzzy algorithm to estimate effective wind speed and optimal rotor speed for variable-speed wind turbine. *Neuro Computing* 272, 495-504.

Bassett, K., R. Carriveau, D. S. K. Ting (2015). 3D printed wind turbines part 1: Design considerations and rapid manufacture potential. *Sustainable Energy Technologies and Assessments* 11, 186-193.

Bekir, A. and S. Reşat (2019). Estimation of Wind Turbine Energy Production Value by Using Machine Learning Algorithms and Development of Implementation Program. *Energy Sources, Part A: Recovery, Utilization, and Environmental Effects* 1631410.

Chen, M. R., G. Q. Zeng, K. D. Lu and J. Weng (2019). A two-layer nonlinear combination method for short-term wind speed prediction based on ELM, ENN, and LSTM. *IEEE Internet of Things Journal* 6(4), 6997-7010.

Deam, R. T. (2008). On scaling down turbines to millimeter size. *Journal of Engineering for Gas Turbines and Power* 130, 52301-52309.

Gohar, G. A., T. Manzoor, A. Ahmad, Z. Hameed, F. Saleem, I. Ahmad, A. Sattar and A. Arshad (2019). Design and comparative analysis of an INVELOX wind power generation system for multiple wind turbines through computational fluid dynamics. *Advances in Mechanical Engineering* 11(4), 1-10.

Guo, Y., Y. Chen, J. Ma, H. Zhu, X. Cao, N. Wang and Z. L. Wang (2019). Harvesting wind energy: a hybridized design of pinwheel by coupling tribo electrification and electromagnetic induction effects. *Nano Energy* 60, 641-648.

Hao, W., Y. M. Zhang, J. X. Mao and H. P. Wan (2020). A probabilistic approach for short-term prediction of wind gust speed using ensemble learning. *Journal of Wind Engineering &*

- Industrial Aerodynamics*, <https://doi.org/10.1016/j.jweia.2020.104198>.
- Hao, Z., D. Niu, M. Yu, K. Wang, Y. Liang and X. Xu (2020). A Hybrid Deep Learning Model and Comparison for Wind Power Forecasting Considering Temporal-Spatial Feature Extraction. *MDPI Sustainability*, 9490.
- Howell, R., N. Qin, J. Edwards and N. Durrani (2010). Wind tunnel and numerical study of a small vertical axis wind turbine. *Renewable Energy* 35(2), 412-422.
- Khan, M., T. Liu and F. Ullah (2019). A new hybrid approach to forecast wind power for large scale wind turbine data using deep learning with Tensor Flow framework and principal component analysis. *Energies* 12(12), 2229.
- Khodayar, M. and J. Wang (2018). Spatio-temporal graph deep neural network for short-term wind speed forecasting. *IEEE Transactions on Sustainable Energy* 10(2), 670-681.
- Kosasih, B. and H. S. Hudin (2016). Influence of inflow turbulence intensity on the performance of bare and diffuser-augmented micro wind turbine model. *Renewable Energy* 87, 154-167.
- Li, W., X. Jia, X. Li, Y. Wang and J. Lee (2021). A Markov model for short term wind speed prediction by integrating the wind acceleration information. *Renewable Energy* 164, 242-253.
- Lin, Z. and X. Liu (2020). Wind power forecasting of an offshore wind turbine based on high-frequency SCADA data and deep learning neural network. *Energy* 201, 117693.
- Zi, L., X. Liu and M. Collu (2020). Wind power prediction based on high-frequency SCADA data along with isolation forest and deep learning neural networks. *International Journal of Electrical Power & Energy Systems* 118, 105835.
- Liu, H., X. Mi and Y. Li (2018). Smart deep learning-based wind speed prediction model using wavelet packet decomposition, convolutional neural network and convolutional long short term memory network. *Energy Conversion and Management* 166, 120-131.
- Liu, H., Z. Zhang, H. Jia, Q. Li, Y. Liu and J. Leng (2020). A novel method to predict the stiffness evolution of in-service wind turbine blades based on deep learning models. *Composite Structures* 252, 112702.
- Liu, Y., H. Qin, Z. Zhang, S. Pei, Z. Jiang, Z. Feng and J. Zhou (2020). Probabilistic spatiotemporal wind speed forecasting based on a variational Bayesian deep learning model. *Applied Energy* 260, 114259.
- Ma, Z., H. Chen, J. Wang, X. Yang, R. Yan, J. Jia and W. Xu (2020). Application of hybrid model based on double decomposition, error correction and deep learning in short-term wind speed prediction. *Energy Conversion and Management* 205, 112345.
- Manwell, J. F., J. G. McGowan and A. L. Rogers (2009). *Wind Energy Explained Theory, Design and Application*. Second Edition, ISBN 978-0-470-01500-1.
- Memarzadeh, G. and F. Keynia (2020). A new short-term wind speed forecasting method based on fine-tuned LSTM neural network and optimal input sets. *Energy Conversion and Management* 213, 112824.
- Ohba, M. (2019). The impact of global warming on wind energy resources and ramp events in Japan. *Atmosphere* 10(5), 265.
- Ramesh Kumar, K. and M. Selvaraj (2023). Investigations on integrated funnel, fan and diffuser augmented unique wind turbine to enhance the wind speed. *Journal of Applied Fluid Mechanics* 16(3), 575-589.
- Shahbazi, R. Sh. Kouravand and R. Hassan-Beygi (2019) Analysis of wind turbine usage in greenhouses: wind resource assessment, distributed generation of electricity and environmental protection. *Energy Sources, Part A: Recovery, Utilization, and Environmental Effects*.
- Sorribes-Palmer, F., A. Sanz-Andres, L. Ayuso, R., Sant and S. Franchini (2017). Mixed CFD-1D wind turbine diffuser design optimization. *Renewable Energy* 105, 386-399.
- Wang, J., Y. Wang and Y. Li (2018). A novel hybrid strategy using three-phase feature extraction and a weighted regularized extreme learning machine for multi-step ahead wind speed prediction. *Energies* 11(2), 321.
- Zhu, X., R. Liu, Y. Chen, X. Gao, Y. Wang and Z. Xu (2021). Wind speed behaviors feather analysis and its utilization on wind speed prediction using 3D-CNN. *Energy* 236, 121523.